Eur. Phys. J. B **9**, 445–459 (1999)

THE EUROPEAN PHYSICAL JOURNAL B

EDP Sciences

Experimental determination and modelization of a unique phase diagram: solid solutions of antiferromagnetic organometallic radical cation salts $[Cp_2Mo(dmit)^{+\bullet}][X^-]_{(x)}[PF_6^-]_{(1-x)}$ ($X^- = AsF_6^-$ or SbF_6^-)

R. Clérac[1,a], M. Fourmigué[2], J. Gaultier[3], Y. Barrans[3], P.A. Albouy[4], and C. Coulon[5,b]

[1] Centre de Recherche Paul Pascal, CNRS, avenue du Dr. Schweitzer, 33600 Pessac, France
[2] Institut Jean Rouxel, CNRS-Université de Nantes, 2 rue de la Houssinière, BP 32229, 44322 Nantes cedex 03, France
[3] Institut de Chimie de la Matière Condensée de Bordeaux, avenue du Dr. Schweitzer, 33600 Pessac, France
[4] Laboratoire de Physique des Solides, CNRS-Université Paris-Sud, Bâtiment 510, 91405 Orsay cedex, France

Received 5 August 1998

Abstract. The physical properties of paramagnetic Mo(V) organometallic radical cation salts, $[Cp_2Mo(dmit)^{+\bullet}][X^-]$, are investigated through the study of two series of solid solutions $[Cp_2Mo(dmit)^{+\bullet}][X^-]_{(x)}[PF_6^-]_{(1-x)}$ incorporating two kinds of anions (AsF_6^-/PF_6^- or SbF_6^-/PF_6^-). The combination of EPR and X-ray diffraction is used to specify the nature of the structural phase transitions which occur in the paramagnetic phase and to determine the corresponding (T, x) phase diagrams. Finally, antiferromagnetic resonance is studied to probe the low temperature antiferromagnetic ground state. In the last part of the paper, the observed complex phase diagram is analyzed by considering a compressible model with at least two independent modes of compression. We conclude that the larger compressibilities are associated with the smaller anions.

PACS. 76.30.-v Electron paramagnetic resonance and relaxation – 61.50.Ks Crystallographic aspects of phase transformations – 75.50.Ee Antiferromagnetics

1 Introduction

In a previous paper [1], hereafter labelled as paper I, a series of three $S = 1/2$ radical cation salts of $Cp_2Mo(dmit)$ were described with the increasingly larger PF_6^-, AsF_6^- and SbF_6^- closed-shell octahedral anions. These three compounds crystallize in the orthorhombic system, space group Cmcm at room temperature. Upon cooling a *second order* structural phase transition at T_1 (PF_6^-: 120 K, AsF_6^-: 142 K, SbF_6^-: 175 K) to a triclinic system is observed, which also reveals a twinning of the crystals. Therefore, the orthorhombic structure can also be described as the combination of two monoclinic elements, as shown in Figure 1. As in paper I, this monoclinic description which allows a simpler description of the physical properties will be used through the following of this paper.

In the three compounds, the structural phase transition which occurs at T_1 is accompanied by the apparition of satellite peaks characteristic of a superlattice of wave vector $\mathbf{q}_1^* = (0, 1/2, 1/2)_{\text{centered}}$. Here, the label "centered" indicates that this superlattice is characterized by the presence of a pseudo-extinction which finds its origin in the pseudo centering of the novel a', b', $c' = a$, $2b$, $2c$ triclinic unit cell. The corresponding diffraction conditions then write: $k' + l' = 2n$. This structural phase transition is also revealed by a drastic increase of the EPR linewidth. At lower temperature, two strikingly different behaviours were found:

- In the AsF_6^- and SbF_6^- salts, the same superlattice is observed down to 10 K from X-ray study although another inflexion point is found in the EPR linewidth temperature dependence.
- In the PF_6^- salt, a *first order* phase transition is found at $T_2 = 89$ K with the appearance of a novel superlattice at a wave vector $\mathbf{q}_2 = (0, 1/2, 0)$. This phase transition is also revealed by a step in the EPR linewitdth.

At still lower temperature all three compounds reach an antiferromagnetic ground state, identified by static susceptibility measurements and antiferromagnetic resonance (AFMR) experiments below the Néel

[a] *Present address*: Department of Chemistry, Michigan State University, East Lansing, Michigan 48824-1128, USA
[b] e-mail: coulon@crpp.u-bordeaux.fr

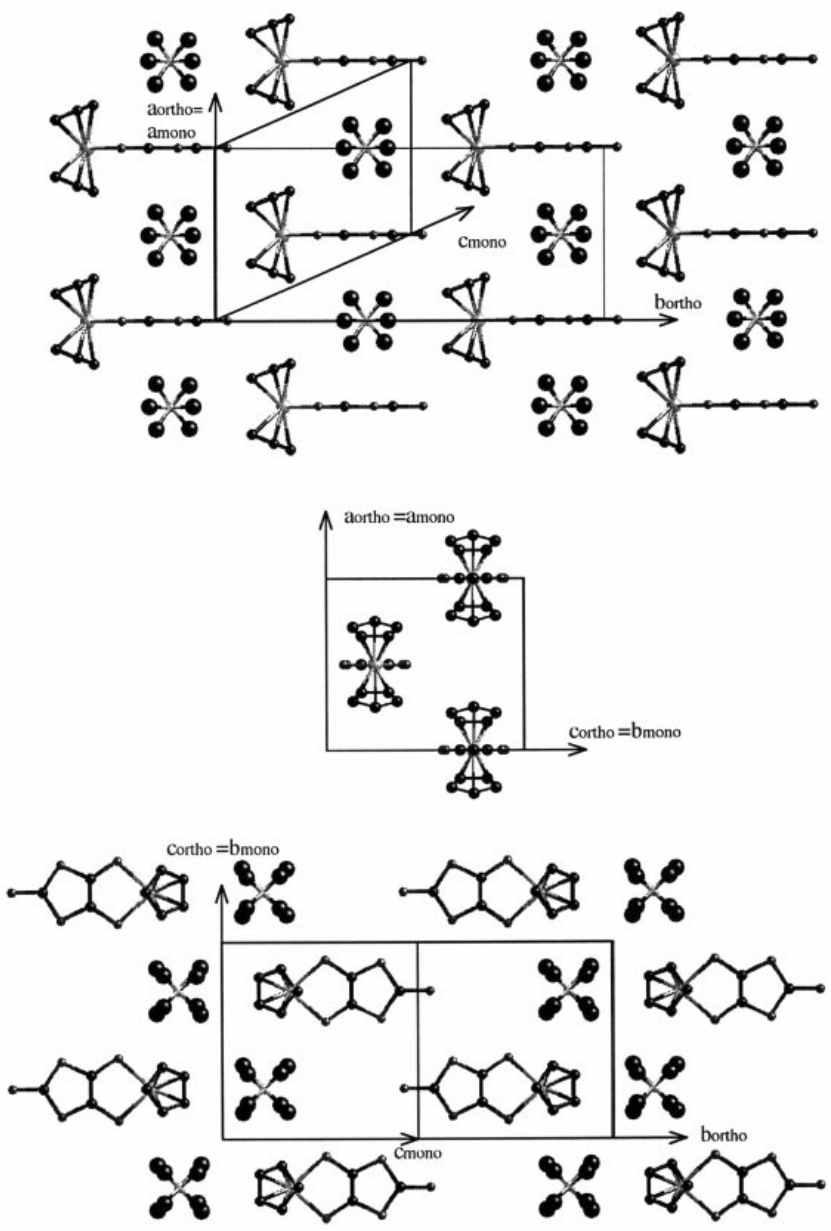

Fig. 1. Comparison of the orthorhombic and monoclinic descriptions of the room temperature crystal structure.

temperature: T_N = 11.5 K, 9.5 K and 7.5 K in the pure PF_6^-, AsF_6^- and SbF_6^- salts respectively. The main question which arises from paper I is the following: why is there such a different behaviour between the PF_6^- salt and the two other compounds? More generally, what is the origin of these structural transitions? Therefore, we have prepared two series of solid solutions $[Cp_2Mo(dmit)^{+\bullet}][X^-]_{(x)}[PF_6^-]_{(1-x)}$ where X^- is AsF_6^- or SbF_6^-. As for the pristine samples, these salts were obtained by electrocrystallization of the neutral $Cp_2Mo(dmit)$ in CH_2Cl_2 solutions of n-$Bu_4N^+X^-$ and n-$Bu_4N^+PF_6^-$ in the desired molar proportions with a total 0.05 M electrolyte concentration, as described for the pure salts [1]. This alloy strategy has been particularly successful in the study of one-dimensional superconductors (Bechgaard salts) such as $(TMTSF)_2(ReO_4)_{(1-x)}(ClO_4)_{(x)}$ [2], $[(TMTSF)_{(1-x)}(TMTTF)_{(x)}]_2ReO_4$ [3] or $(TMTTF)_2(X)_{(1-x)}(PF_6)_{(x)}$ (with X^-: AsF_6^- or SbF_6^-) [4].

The complete study of the corresponding binary phase diagrams is expected to provide pertinent informations on the evolution of the physical properties with x through combined EPR and low temperature X-ray experiments. These results, together with antiferromagnetic resonance data, are described in the experimental part of the paper. The last part will be devoted to the discussion of the experimental phase diagrams, mostly through symmetry arguments and Landau theory.

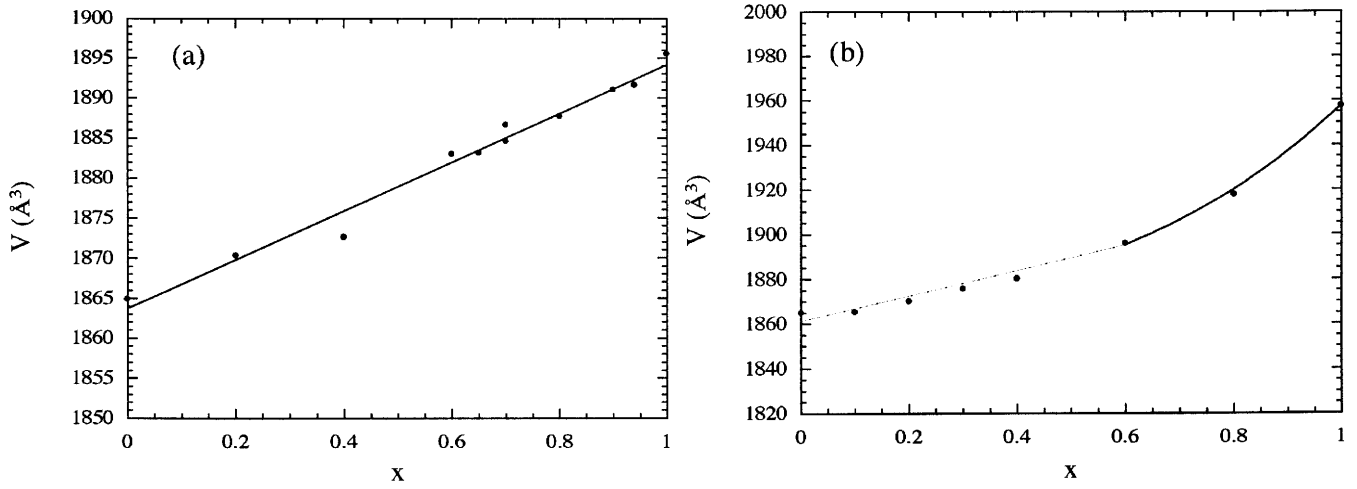

Fig. 2. Effect of alloying on the volume of the unit cell; (a) PF_6^-/AsF_6^-, (b) PF_6^-/SbF_6^- alloys.

2 Experimental results

2.1 Structural characterization

As a first structural characterization, the room temperature unit cell of the different solid solutions has been determined. All samples are isostructural with the pristine salts and exhibit unit cell parameters which evolve continuously between those of the pure salts. Figure 2 gives the evolution of the unit cell volume for the two series. The linear dependence obtained in the case of the AsF_6^-/PF_6^- alloys (Fig. 2a) suggests a random mixing of the two kinds of anions in the solid. Accordingly, these series of solid solutions will be compared in the following with the pristine salts considering that $[Cp_2Mo(dmit)^{+\bullet}][AsF_6^-]_{(x)}[PF_6^-]_{(1-x)}$ is equivalent to a pure sample with an anion of intermediate size. Figure 2b shows that the same assumption is also valid in the $[Cp_2Mo(dmit)^{+\bullet}][SbF_6^-]_{(x)}[PF_6^-]_{(1-x)}$ series as long as x is smaller than 0.5 (this will be the most interesting part of the phase diagram in the following).

2.2 EPR results

It has been shown in paper I that EPR is relevant to probe the low temperature properties of these materials. Indeed, the EPR linewidth temperature dependence is the easiest way to locate the structural phase transitions [5–7] and to specify their second or first order character. We therefore use the same technique to study the two series of solid solutions.

Temperature dependence of the EPR linewidth of $[Cp_2Mo(dmit)^{+\bullet}][AsF_6^-]_{(x)}[PF_6^-]_{(1-x)}$ for six selected x values are given in Figure 3. Qualitatively, the same behaviour, reminiscent of the one found for the pure $[Cp_2Mo(dmit)^{+\bullet}][PF_6^-]$, is observed for all x values, even up to $x = 0.99$ (*i.e.* 1% PF_6^- in the pure AsF_6^- salt): an inflexion point at a temperature T_1, a sharp decrease of the linewidth at T_2 and finally a precursor effect close to the Néel temperature T_N. These temperatures for the different alloys are given in Table 1. Note that the pure AsF_6^- salt is the only one to exhibit a single structural phase transition at T_1. By analogy with the pure salts, and anticipating the X-ray study, the sharp decrease of the EPR linewidth at T_2 suggests the occurrence of a first order transition. Thus, our data imply a line of first order transitions as x goes from 0 to 0.99. We know however from paper I that this phase transition does not exist at $x = 1$ (for the pure AsF_6^- salt) and the question of how this line ends near $x = 1$ remains open.

Experimentally, it is hopeless to prepare with enough accuracy samples with x between 0.99 and 1. We can however investigate more closely the linewidth EPR discontinuity at T_2 as a function of x. Indeed, for a first order phase transition, we expect the amplitude of the linewidth jump to be a relevant information. Accordingly, we plot in Figure 4 the normalized linewidth jump $(\Delta H_{max} - \Delta H_{min})/(\Delta H_{max} + \Delta H_{min})$ observed at T_2 as a function of x. Two different regimes are found. First, a slight increase with a maximum for $x \approx 0.9$; then a strong decrease for $0.9 \leq x \leq 0.99$. This result suggests a crossover close to $x = 0.9$. This would mean that the first order character of the transition decreases rapidly as x approaches 1 as it is expected if the first order line ends with a liquid/gaz-like critical point. Within this scenario, the localization of this critical point close to $x = 1$ would be totally accidental and not related to a possible disorder effect due to the anion substitution.

In order to test this assumption, a new series of solid solutions incorporating the PF_6^- and SbF_6^- anions were prepared. Since the SbF_6^- anion is notably larger than the AsF_6^- one, we expect a shift of the critical point to a smaller x value in the PF_6^-/SbF_6^- phase diagram. The EPR linewidth of selected $[Cp_2Mo(dmit)^{+\bullet}][SbF_6^-]_x[PF_6^-]_{(1-x)}$ solid solutions are given Figure 5. In this new series, the "PF_6^- like" behaviour is only observed below $x_c = 0.35$, while a temperature dependence similar to the one found for the pure SbF_6^- or AsF_6^- salts is found above $x_c = 0.35$. The characteristic temperatures deduced from these data are given in Table 2. As anticipated, the substitution of SbF_6^- for AsF_6^- allowed us to indeed expand the phase diagram and

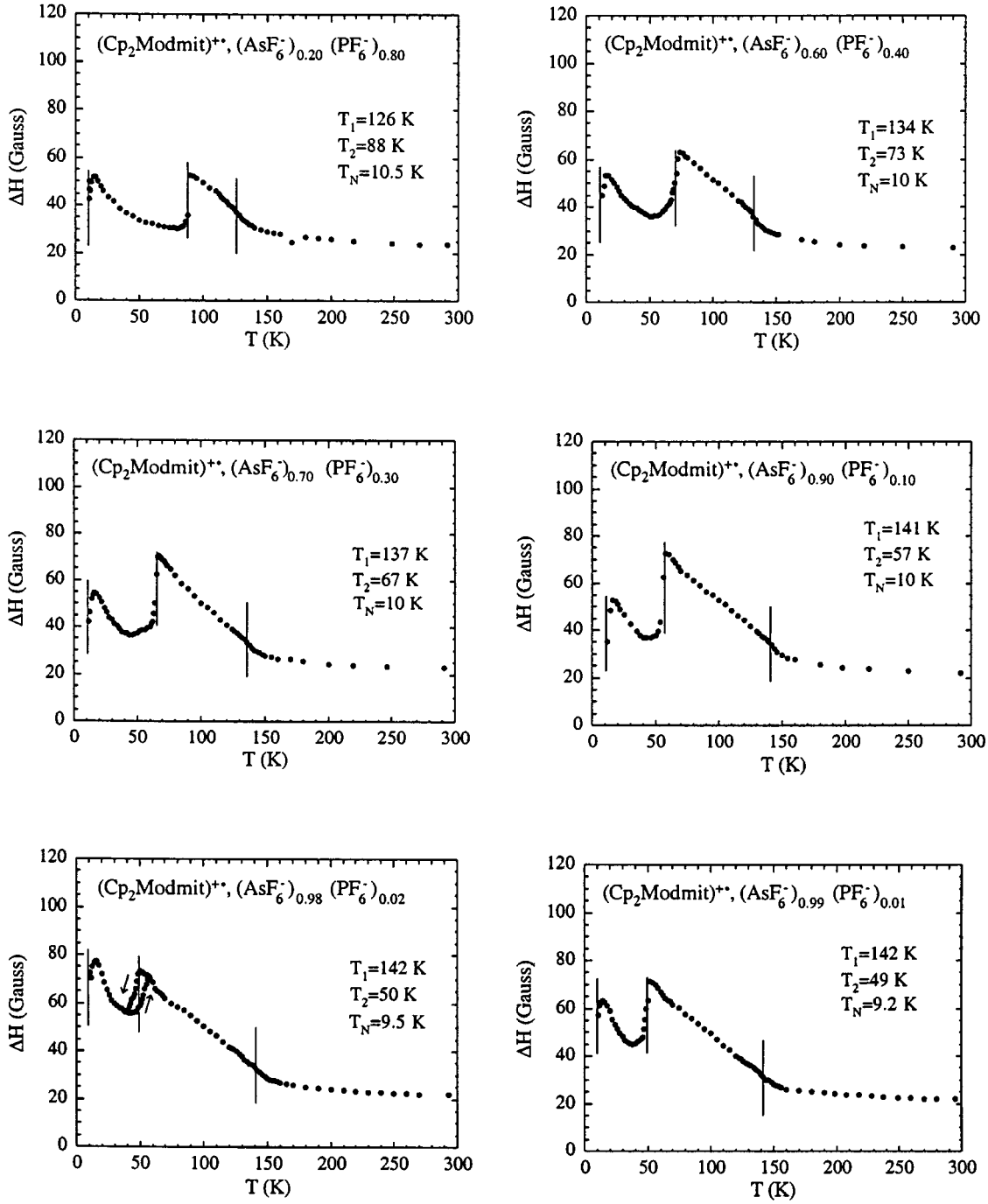

Fig. 3. Temperature dependence of the EPR linewidth in the $[Cp_2Mo(dmit)^{+\bullet}][AsF_6^-]_{(x)}[PF_6^-]_{(1-x)}$ series with the magnetic field applied in the c^* direction.

hence to shift the critical point far away from the borders ($x = 0$ or $x = 1$).

For $x \leq 0.35$, the first order character of the phase transition is analyzed through the evolution of the normalized linewidth jump (Fig. 6). A crossover is now observed around $x = 0.24$ and the drop found close to x_c is also in favor of a critical point. Thus, we confirm the analogy with the first PF_6^-/AsF_6^- solid solutions and conclude that the topology of the two phase diagrams is similar. X-ray data are now necessary to confirm the character of the phase transitions and to determine the nature of the different phases involved.

2.3 Low-temperature X-ray studies

Because of the analogy between the two series, this study was only developed on the PF_6^-/AsF_6^- solid solutions. As for the pure samples, this work has been performed on

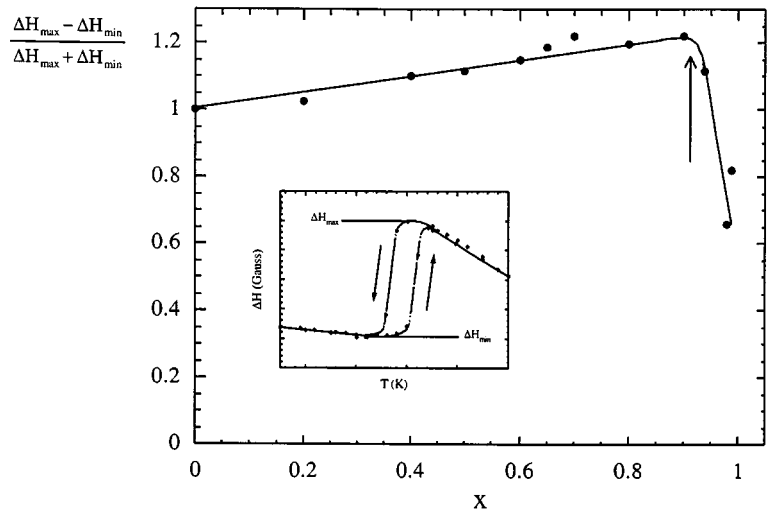

Fig. 4. Normalized EPR linewidth jump at T_2 in the $[Cp_2Mo(dmit)^{+\bullet}][AsF_6^-]_{(x)}[PF_6^-]_{(1-x)}$ series.

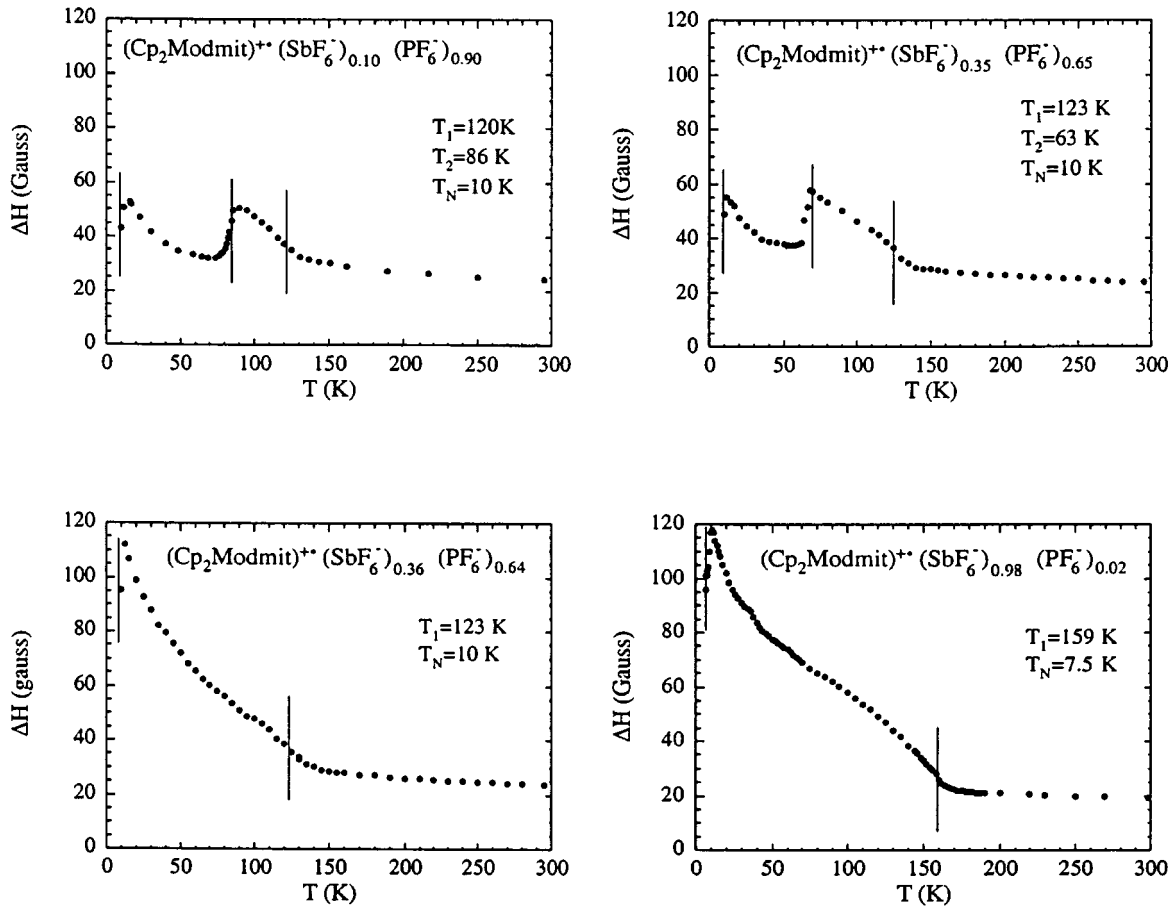

Fig. 5. Temperature dependence of the EPR linewidth in the $[Cp_2Mo(dmit)^{+\bullet}][SbF_6^-]_{(x)}[PF_6^-]_{(1-x)}$ series with the magnetic field applied in the c^* direction.

Table 1. Cell parameters, phase transition temperatures and AFMR experimental parameters (defined in the text, see 2.5) of the solid solutions $[Cp_2Mo(dmit)^{+\bullet}][AsF_6^-]_{(x)}[PF_6^-]_{(1-x)}$.

x	a (Å)	b (Å)	c (Å)	V (Å^3)	T_1 (K)	T_2 (K)	T_N (K)	B_-(Gauss)	B_+(Gauss)	$2\theta(^\circ)$	$I[B_2]/I[B_1]$
$Cp_2Mo(dmit)PF_6$	8.954(1)	20.596(3)	10.112(3)	1864.9(6)	120	89	10.5	6200	7000	18	0
0.20	8.950(1)	20.623(3)	10.133(3)	1870.3(6)	126	88	10.5			18	0
0.40	8.958(1)	20.612(8)	10.142(1)	1872.6(8)	130	83	10.3	6200	7000	18	0
0.50					133	78	10			18	0
0.60	8.968(1)	20.646(3)	10.168(5)	1883.0(8)	134	73	10	6200	7000	18	0
0.65	8.969(1)	20.640(4)	10.173(3)	1883.1(8)			10	6300	7000	18	0.4
								6200	7400	70	
0.70	8.972(1)	20.661(3)	10.177(2)	1886.6(5)	137	67	10			18/70	0.55
0.80	8.972(2)	20.657(5)	10.185(4)	1887.7(9)	140	65	10			18/70	0.6
0.90	8.969(2)	20.660(7)	10.206(5)	1891.0(9)	141	57	10	6300	7000	18	0.8
								6100	7400	73	
0.94	8.983(1)	20.619(3)	10.213(5)	1891.6(9)	142	54	9.5			18/75	0.7
0.98					142	50	9.5	6200	7000	18	3.8
								6200	7400	77	
0.99					142	49	9.2	6200	7200	18	2.6
								5800	7300	78	
								6700	7900	78	
$Cp_2Mo(dmit)AsF_6$	8.9779(9)	20.647(2)	10.225(1)	1895.5(3)	142		9.2	6000	7200	78	∞

Table 2. Cell parameters and phase transition temperatures of the solid solutions $[Cp_2Mo(dmit)^{+\bullet}][SbF_6^-]_{(x)}[PF_6^-]_{(1-x)}$.

x	a (Å)	b (Å)	c (Å)	V (Å^3)	T_1 (K)	T_2 (K)	T_N (K)
$Cp_2Mo(dmit)PF_6$	8.954(1)	20.596(3)	10.112(3)	1864.9(6)	120	89	10.5
0.10	8.955(1)	20.612(1)	10.101(4)	1864.3(8)	120	86	10.0
0.20	8.956(1)	20.605(2)	10.133(4)	1870.0(8)	120	72	10.0
0.30	8.962(1)	20.612(3)	10.154(2)	1875.7(5)	120	66	10.0
0.34					120	61	10.0
0.35					123	63	10.0
0.36					123		10.0
0.40	8.969(1)	20.613(3)	10.159(2)	1878.1(6)	125		9.5
0.80	9.017(1)	20.703(2)	10.273(3)	1917.7(7)	138		8.0
0.98					159		7.5
$Cp_2Mo(dmit)SbF_6$	9.056(1)	20.816(4)	10.383(3)	1957.4(7)	175		7.5

Weissenberg photographs obtained from an home-made diffractometer allowing a temperature control between 300 and 10 K. Experimental details are given in paper I. Only representative solid solutions have been studied, they are mentioned in Table 1.

Let us first recall the main results obtained for the pure PF_6^- and AsF_6^- salts. In both compounds, a second order phase transition is observed upon cooling at T_1. A superlattice is stabilized below this temperature with a wave vector $\mathbf{q}_1^* = (0, 1/2, 1/2)_{\text{centered}}$ (using the monoclinic description above T_1). Here the index "centered" indicates that pseudo-extinctions are found although no real extinction is expected in the low temperature triclinic system. This means a very small (*i.e.* not detectable) intensity for some reflexions of the low temperature reciprocal lattice. More precisely, the Bragg spots with $h' + l' = 2n$ (where n is an integer and h', k', l' are the Miller indices of the new triclinic lattice) are not detected. We will see in the following the importance of this result to discuss the phase diagram. At a lower temperature T_2, a first order phase transition is found for the PF_6^- salt. It corresponds to a discontinuous evolution of the wave vector of the superlattice which becomes $\mathbf{q}_2 = (0, 1/2, 0)$ below T_2. As far as the T_1 second-order phase transition is concerned,

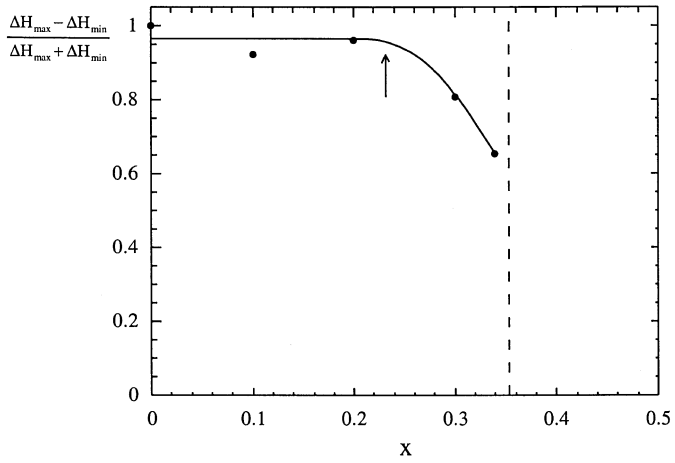

Fig. 6. Normalized EPR linewidth jump at T_2 in the $[Cp_2Mo(dmit)^{+\bullet}][SbF_6^-]_{(x)}[PF_6^-]_{(1-x)}$ series.

the behaviour of the solid solutions is similar to the one found for the pristine samples. This was expected from EPR experiments which give a continuous extrapolation of T_1 between the PF_6^- and the AsF_6^- salts. The results are however more complex at lower temperature. The solid solutions with $x = 0.6$, 0.7 and 0.9 behave qualitatively like the pure PF_6^- salt. First, a second-order transition at T_1 leads to a triclinic system with a $\mathbf{q}_1^* = (0, 1/2, 1/2)_{\text{centered}}$ superlattice. This order disappears totally at T_2 where a first-order transition gives rise to the novel $\mathbf{q}_2 = (0, 1/2, 0)$ superlattice. This behaviour is illustrated in Figures 7a, b, c. In any case, the deduced temperatures for the phase transitions are in agreement with the EPR measurements. The small difference is due to a less accurate temperature determination in the X-ray experiments.

For $x = 0.92$, as shown in Figure 7d, the "centered" $\mathbf{q}_1^*$ superlattice also appears at T_1, but a different behaviour is observed below this temperature. As an example, a "pseudo-extincted" reflexion ($h' + l' = 2n$ with $n = 0$) such as the $(4, 1, \bar{4})$ spot is almost undetectable above 60 K while between 60 and 40 K, it becomes observable and its intensity increases as T decreases. In the same temperature range, the intensity of the observed $(4, 1, \bar{5})$ spot saturates. At $T_2 \approx 40$ K both intensities present a discontinuity. However, none of them goes to zero and the wave vector of the superlattice remains the same, *i.e.* $(0, 1/2, 1/2)$ down to 10 K. Thus, a new kind of first order phase transition is observed at T_2, between two phases of the same symmetry, *i.e.* with the same superlattice $(0, 1/2, 1/2)$ ($\mathbf{q}_1$). None of them is strictly "centered" close to T_2, although we observe a phase transition between a "quasi-centered" phase and a phase where all Bragg spots are present. Therefore, the $\mathbf{q}_1^* = (0, 1/2, 1/2)_{\text{centered}}$ superlattice is simply a limit found in some parts of the phase diagram.

At this point of the presentation, the most important conclusion is the confirmation of the two transition lines suggested by EPR data. The first one is a second-order transition line at T_1 which is present for all the samples. It corresponds to the condensation of the $\mathbf{q}_1^* = (0, 1/2, 1/2)_{\text{centered}}$ superlattice. The second one is a first-order line at T_2. The new important result is that its nature changes around $x^* = 0.9$. Below this value one observes under cooling a transition towards the new $\mathbf{q}_2 = (0, 1/2, 0)$ superlattice. Above x^*, we rather obtain a first-order phase transition between two phases with the same superlattice wave-vector $(0, 1/2, 1/2)$. Note that this crossover around x^* has been already mentionned from the analysis of the EPR linewidth jump at T_2.

2.4 Deduced phase diagrams

From the combined EPR and X-ray data, a phase diagram can be now deduced for both series of solid solutions. First, the location of the second-order line at T_1 which corresponds to the condensation of the $\mathbf{q}_1^* = (0, 1/2, 1/2)_{\text{centered}}$ superlattice has been determined. Moreover, the nature of the first order line at T_2 already detected from EPR has been characterised by the X-ray study in the AsF_6^- series.

Let us first consider the $[Cp_2Mo(dmit)^{+\bullet}][AsF_6^-]_{(x)}[PF_6^-]_{(1-x)}$ salts. As the low temperature superlattice changes at x^*, we expect another transition line to separate below T_2 the two corresponding phases [8]. This line has not be directly observed either with EPR or from X-ray studies although x^* corresponds to the crossover concentration discussed from Figure 4. This suggests that this line may be approximately vertical. Moreover, its nature is the same as the transition line found at T_2 for $x < x^*$ and thus probably a first-order line. The collection of all these data gives the phase diagram shown in Figure 8a where the symmetry of the different phases has been indicated. Note also that the $(0, 1/2, 1/2)$ superlattice is "centered" in most of the temperature domain lying between T_1 and T_2.

A similar analysis can be made for the $[Cp_2Mo(dmit)^{+\bullet}][SbF_6^-]_{(x)}[PF_6^-]_{(1-x)}$ series. In this case, low temperature X-ray data are not available. However, the topology of the phase diagram (Fig. 8b) is clearly similar to the previous series. Furthermore, from Figure 6, we can estimate x^* around 0.24 and we have located the end of the first order line at $x_c = 0.35$. As in the previous case, the evolution of the normalized linewidth jump (Fig. 6) suggests that the first-order line ends with a liquid/gaz-like critical point at x_c.

We finally propose a unique phase diagram for the two series (Fig. 9). Besides the high temperature phase (phase I in the figure), three other phases are found. Two of them (phases II and IV) have the same symmetry and exhibit the same $(0, 1/2, 1/2)$ superlattice ($\mathbf{q}_1$ or $\mathbf{q}_1^*$). They are not qualitatively different but we use two different labels to emphasize the special case of "pseudo-extinctions" (pseudo-centered limit: phase II). The third one, phase III corresponds to the $\mathbf{q}_2 = (0, 1/2, 0)$ superlattice. This very striking topology presents a clear analogy with the phase diagram of a simple pure compound [9]. Indeed, the analogs of phases II and IV would be respectively the gas

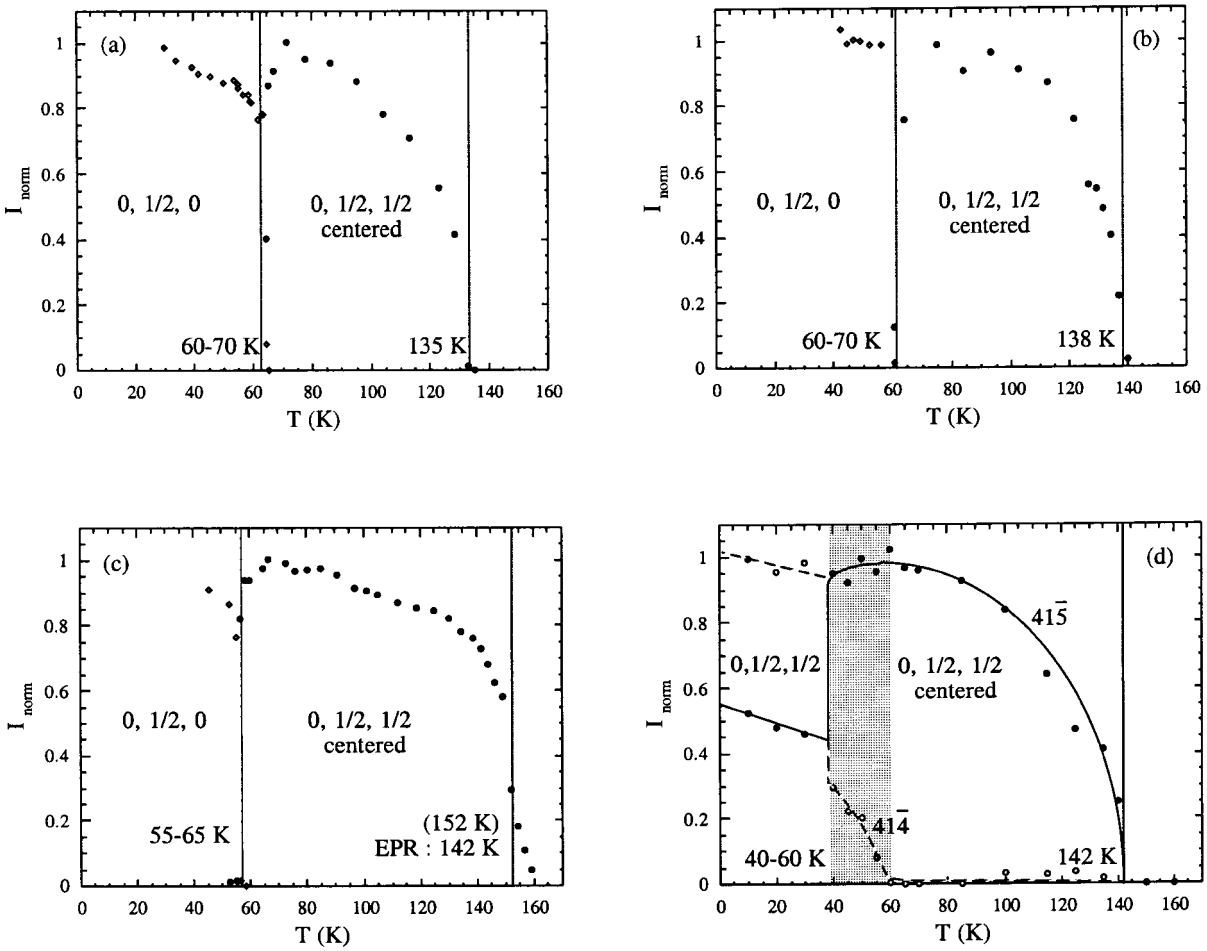

Fig. 7. Temperature dependence of X-ray satellite spots intensity (normalized at saturation) in the $[Cp_2Mo(dmit)^{+\bullet}][AsF_6^-]_{(x)}[PF_6^-]_{(1-x)}$ series; (a) $x = 0.6$, (b) $x = 0.7$, (c) $x = 0.9$, (d) $x = 0.92$.

and the liquid. Both phases belong to the fluid domain and the ideal gas is a special limit where the mass density goes to zero. A first-order line separates an ideal gas from a dense liquid far from the critical point. This lines ends at the critical point where both fluids have the same density. Phase III would be the analog of the solid phase. We propose in the last part of this paper a quantitative discussion of this phase diagram and its analogy with the gaz/liquid/solid problem.

2.5 Antiferromagnetic resonance

As for the pristine salts antiferromagnetic resonance (AFMR) gives information on the magnetic parameters below the Néel temperature. Details on the experiment are given in paper I. By rotating single crystals in simple crystallographic planes, characteristic rotation patterns (giving the resonance field as a function of the rotation angle) are obtained. In the present work, we will essentially discuss the PF_6^-/AsF_6^- series and compare rotation patterns in the (bc^*) plane. Selected data are given in Figures 10a-d.

For $x = 0.4$ (Fig. 10a), two "bubbles" are found, as observed previously for the pure PF_6^- salt. Each of them is characteristic of AFMR when the experimental frequency is smaller than Ω_- [10]. The extremum corresponds to the easy axis. As for the pristine salts, the presence of two bubbles confirms the twinning of the crystals. However, the figure becomes more complex as x increases. Figures 10b and 10c show that four bubbles are observed when x is close to 0.9 (in fact above 0.65). The complexity increases for x close to $x = 1$. For example, Figure 10d shows that three pairs of bubbles are observed for $x = 0.99$. As in paper I, we have fitted these results using the AFMR theory [11,12]. All fits were made in the low temperature limit ($r = 1$) and the two remaining parameters are B_- and B_+ (proportional to the characteristic frequencies Ω_- and Ω_+). The continuous lines give the best fits in Figures 10a-d. Moreover, we also deduce the angle 2θ between the extrema of the two members of a pair (which have identical values of B_- and B_+). When two (three as in Fig. 10d) pairs are present, we deduce two (three) groups of parameters, given in Table 1. Let us discuss the data. Firstly, the anisotropy parameters B_- and B_+ have similar values among the series. This is not surprising since

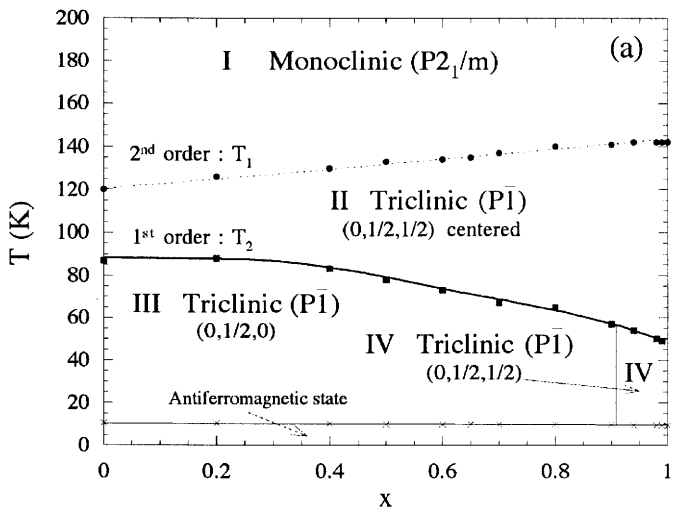

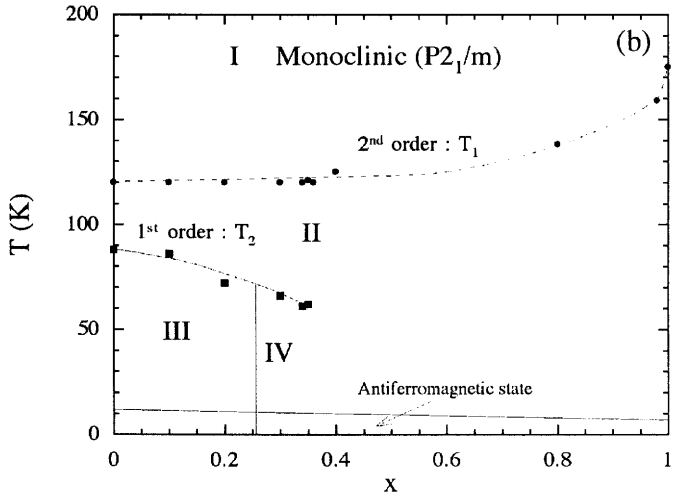

Fig. 8. Deduced phase diagram; (a) in the $[Cp_2Mo(dmit)^{+\bullet}][AsF_6^-]_{(x)}[PF_6^-]_{(1-x)}$ series, (b) in the $[Cp_2Mo(dmit)^{+\bullet}][SbF_6^-]_{(x)}[PF_6^-]_{(1-x)}$ series.

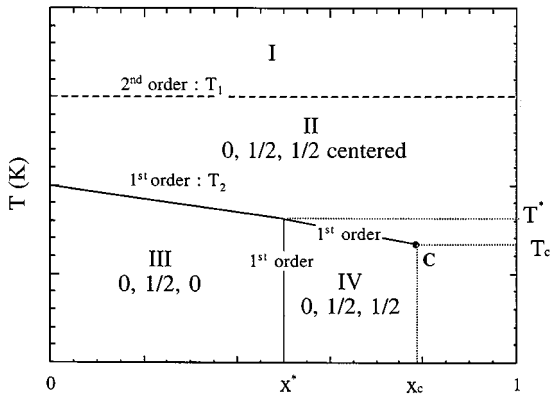

Fig. 9. Schematic phase diagram obtained from the experimental studies of the two solid solution series.

the pristine salts also have very similar parameters. However, the differences are large enough to give different shapes to the bubbles. For the pristine salts, the extrema of the resonance field are roughly (3000 G - 9200 G) and (3200 G - 7800 G) for the PF_6^- and AsF_6^- salts respectively. As shown in Figure 10a, up to $x = 0.6$, the pair of bubbles (B_1) is similar to the one observed for the pure PF_6^- salt. The separation between the two patterns is also the same $2\theta = 18°$. Above this concentration ($x > 0.6$), the first pair is still present with the same 2θ separation but a new pair of bubbles (B_2) appears with different extrema (4000 G - 8500 G) and a separation which depends on the AsF_6^- concentration (see Fig. 11a). For $x = 0.99$ (Fig. 10d), a weak third pair appears besides these two pairs, very similar to the one observed for the pure AsF_6^- salt. This more complex behaviour which remains marginal among the series may be due to the presence of small domains of pure AsF_6^- in the sample. Ignoring this complication, we have plotted as a function of x the relative intensity of the resonance lines related to B_2 and B_1 (Fig. 11b). Although this ratio always increases with the AsF_6^- concentration, a crossover is found close to $x = 0.92$ where the superlattice wave-vector of the low temperature phase is expected to change. Above this concentration the angle separation between the B_2 pair increases more rapidly to reach continuously the value for the pure AsF_6^- salt ($2\theta = 78°$). This crossover may be associated with the presence of the vertical first order transition line mentioned above albeit no discontinuity can be observed in Figure 11 around $x = 0.92$.

3 Discussion

The combined X-ray and magnetic studies indicate structural phase transitions. As the room temperature crystal structure shows that the anions are disordered (two statistical positions are found: see paper I) it is natural to assume that the anions are involved in the mechanism of these phase transitions. However, because of the twinning of the crystals, we do not know the low temperature structure and the discussion will mostly rely on symmetry arguments. To support these arguments, we will make use of a simple model, whose aim is not to speculate about the nature of the molecular displacements but rather to illustrate the symmetry arguments.

To modelize the low temperature structures, we focus on the anion positions for which we assume (in agreement with structural data) two possible orientations labelled A and B. These two orientations are given in Figure 12. The quantitative modelisation requires the introduction of interactions between pairs of "pseudo-spins" which mimic the orientation degrees of freedom of the anions. As the two possible superlattices have no component in the a direction, a schematic representation is given in Figure 13a only in the (bc) plane. Note that four different coupling constants (J_i with $i = 1$ to 4) have to be defined to describe all first-neighbours interactions.

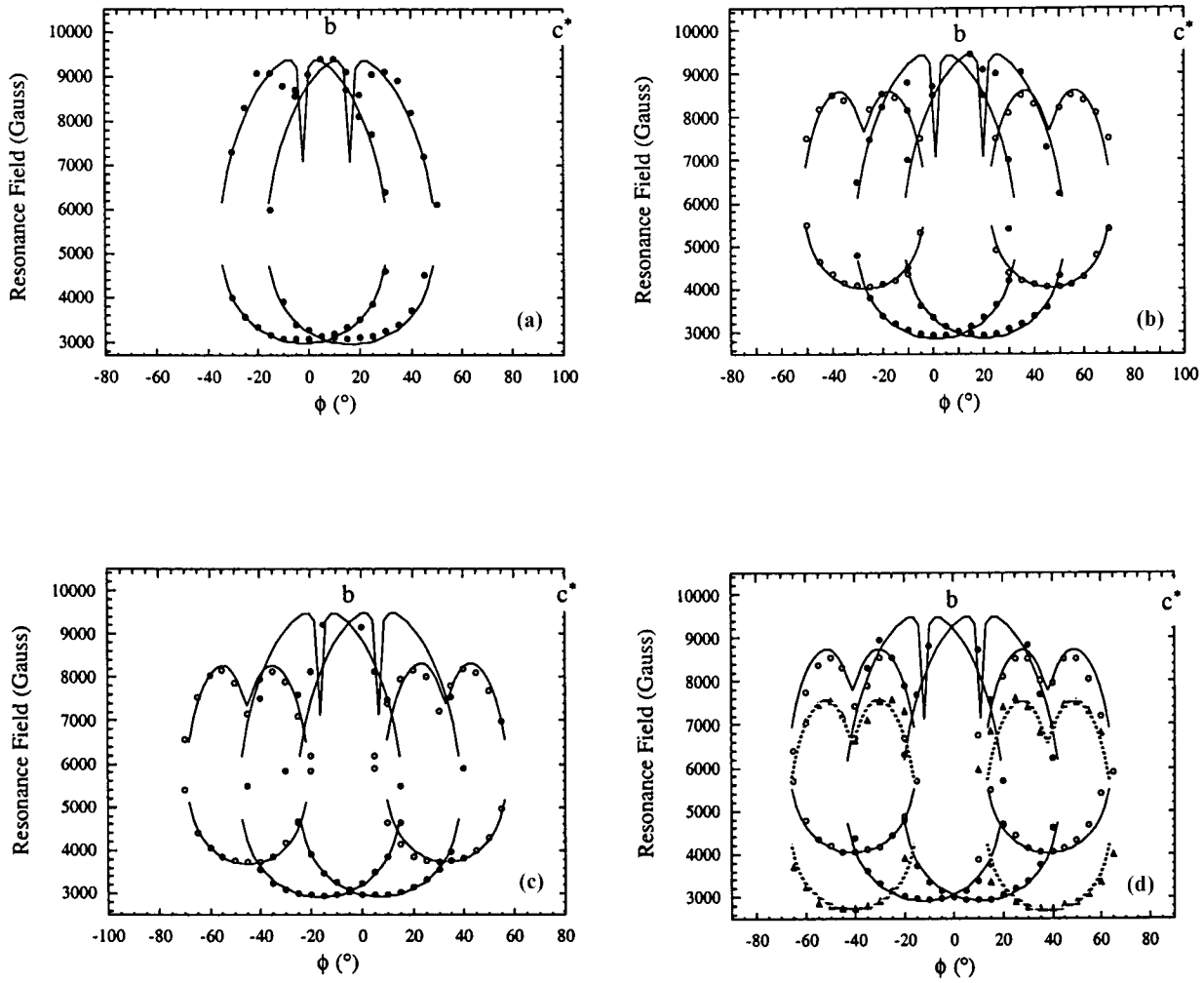

Fig. 10. AFMR rotation pattern in the (bc^*) for the $[Cp_2Mo(dmit)^{+\bullet}][AsF_6^-]_{(x)}[PF_6^-]_{(1-x)}$ series; (a) $x = 0.4$, (b) $x = 0.9$, (c) $x = 0.98$, (d) $x = 0.99$. The continuous and dashed lines gives the fit with the AFMR theory [11,12].

3.1 Need for a compressible model

The above description has been extensively used for example in the context of magnetic phase transitions [13]. Usually the underlying lattice is assumed to be rigid. This is the so-called uncompressible Ising model which predicts a second-order magnetic ordering [9]. If a finite but small compressibility of the lattice is introduced, the results are qualitatively similar. It is only above a critical value of the compressibility that a first order phase transition is predicted [14,15].

In the present case, the problem is different. Figure 13b shows a possible ordered state with a doubling of the unit cell along the b axis, corresponding to the (0, 1/2, 0) superlattice. Because of the symmetry of the high temperature phase, there is a perfect cancellation between the two J_1 or J_2 terms (*i.e.* the A-A and A-B interactions are just opposite terms). If one imagines a small distortion of the lattice which removes this degeneracy, the gain of interaction energy is proportional to the amplitude of the distortion as the loss for the lattice elastic energy is only quadratic. It is therefore always favorable to lower the lattice symmetry when the anions get ordered. This means that the model for the structural distortions is *necessarily compressible*. This argument explains why the crystal structure becomes triclinic below T_1 with unit cell parameters changing rapidly below the phase transition (see paper I).

3.2 How to describe the lattice distortion

As previously mentioned, compressible models are sometimes considered. In these models the lattice distortion is a secondary order parameter coupled to the primary magnetic order parameter. We show in the following that the present problem is specific as two independent secondary order parameters should be considered.

We can illustrate this argument with a simple model. Starting from Figure 13a, we first consider the anion ordering without introducing any lattice distortion. The only information to specify is therefore the state (A or B) for

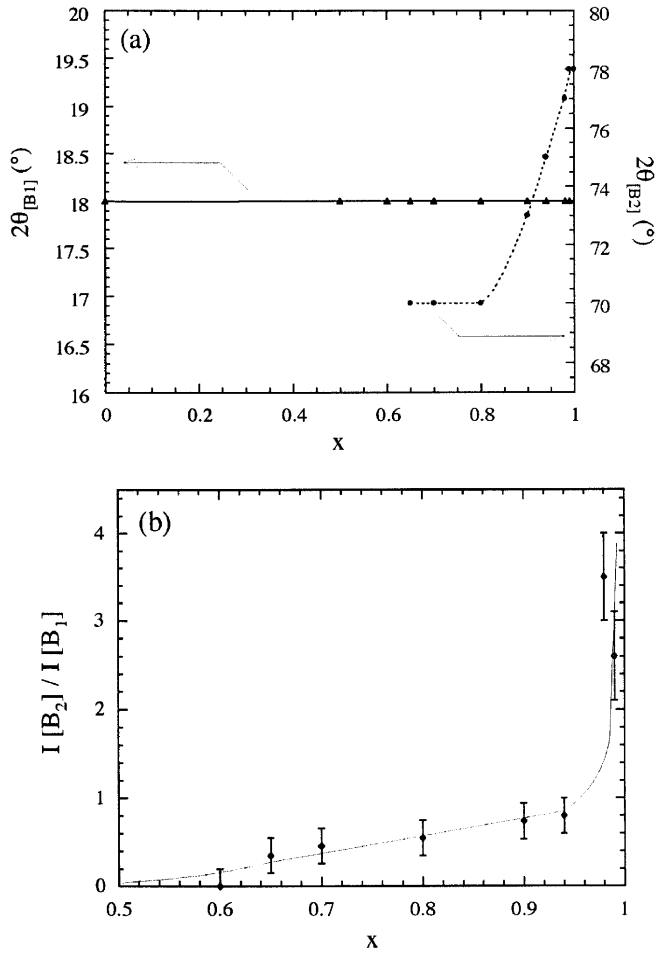

Fig. 11. (a) Angle separation (2θ) between each pair of bubbles, (b) relative intensity between B1 and B2 (internal and external bubbles, see Fig. 10 and text).

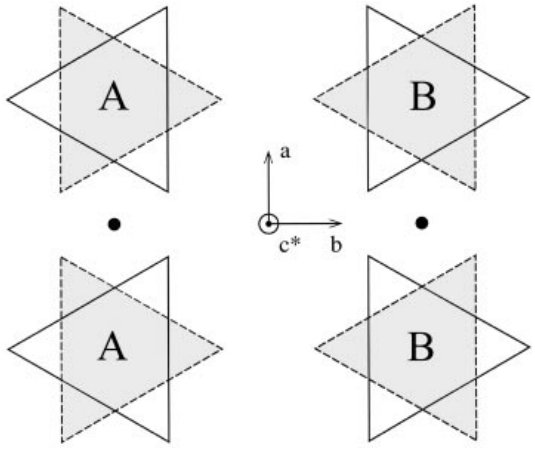

Fig. 12. The two possible orientations (A and B) of the octahedral anions, invariance by inversion (• = inversion center).

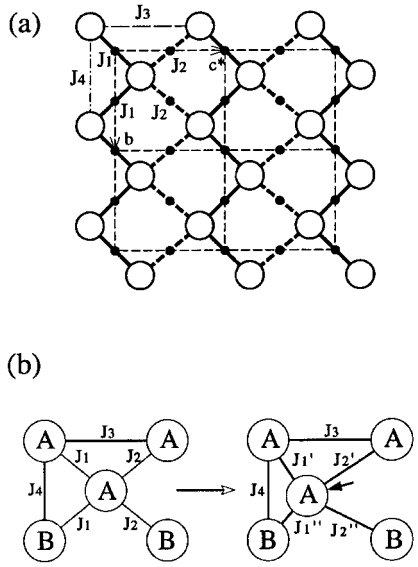

Fig. 13. (a) Illustration of the pair interactions between anions, (b) a possible ordered state to show the cancellation between J_1 or J_2 terms.

every site. The result is given in Figures 14a and 14b respectively for the (0, 1/2, 0) and (0, 1/2, 1/2) superlattice. The centers of symmetry are shown as black dots. Note from Figure 12b that anions which are related by a center of symmetry are in the same state (A or B). We should now introduce a lattice distortion. Any kind of displacement which removes the degeneracy discussed above is acceptable to point out symmetry arguments. For example, we have chosen to rotate centrosymmetric pairs of anions. Figures 14c and 14d give the obtained result respectively for the (0, 1/2, 0) and (0, 1/2, 1/2) superlattice. In this description, the rotation angles play the role of secondary order parameters.

Let us first discuss the (0, 1/2, 0) case (Fig. 14c). Only one angle is required to describe the distortion. As in most of the compressible problems only one secondary order parameter should be introduced. If we now consider the (0, 1/2, 1/2) superlattice (Fig. 14d) and because of the larger unit cell, up to three different independent angles can be introduced. We can go deeper in this discussion taking profit of selected experimental results. First, X-ray data show that the (0, 1/2, 1/2) superlattice is "centered" in the domain II (see Fig. 9). We can in fact produce this special situation in our model choosing $\alpha_1 = \alpha_2$ and $\alpha_3 = 0$. The corresponding molecular organization is given in Figure 15a. In this figure the "pseudo-centers" are shown: they are not imposed by the crystal symmetry but are rather a consequence of special values of the distortion angles. Let us now consider the AFMR data. As the anisotropy is obtained by a summation of dipolar interactions between the spins, the characteristics of the AFMR are mainly sensitive to the local organization of the phase [16]. In that respect, the continuity observe when going from $x = 0.9$ (phase III) to $x = 0.92$ (phase IV) implies that the local order is similar in the two cases although the long range organization is different. In other

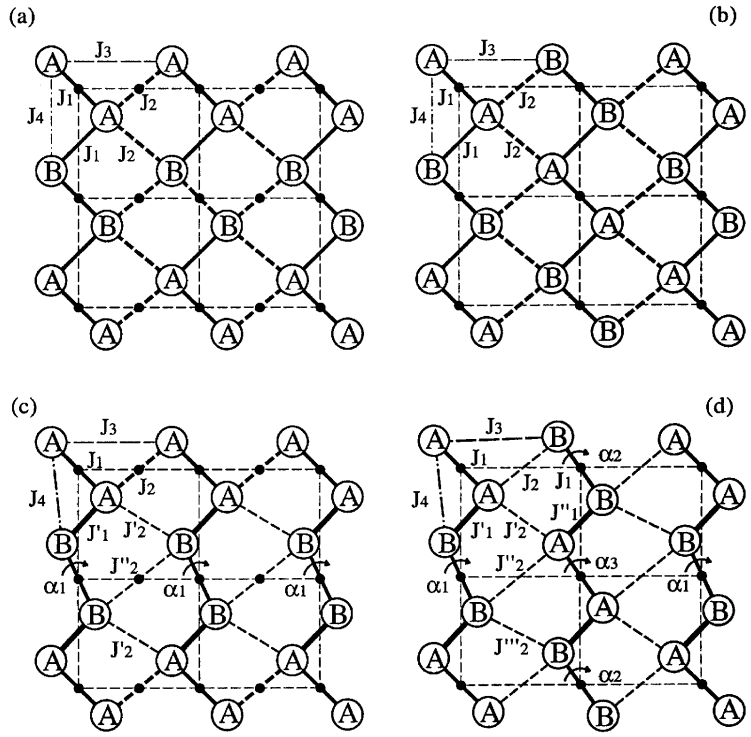

Fig. 14. (0, 1/2, 0) (a) and (0, 1/2, 1/2) (b) ordering in an incompressible model. (c) and (d): same as (a) and (b) respectively when a distortion is introduced.

words, the molecular positions should be similar at the local scale at low temperature in phases III and IV. This conclusion is also in agreement with EPR data which do not allow us to discriminate between the II-III and the II-IV phase transitions (similar values of the EPR linewidth are found in phases III and IV). This remark brings more importance to the analogy with the phase diagram of a simple pure compound: in fact the local order is similar in a liquid and a solid (the mass density is also similar) although the long range order is different. Following our simple modelization, we are now looking for another special organization of the (0, 1/2, 1/2) superlattice close to the one shown in Figure 14c for the (0, 1/2, 0) order. Figure 15b gives the answer: it is obtained when $\alpha_1 = \alpha_3$ and $\alpha_2 = 0$. Finally, to extrapolate between the two extreme situations shown in Figure 15, one should consider at least two independent angles, *i.e. two independent secondary order parameters.*

3.3 Landau theory of the phase diagram

The aim of the preceding discussion was not to imagine a realistic microscopic model but rather to point out the necessary ingredients of any model. In the frame of the Landau theory, we want to determine the free energy as a function of the relevant order parameters. In this description, one free energy is associated to each kind of superlattice, the "optimum wave-vector" being determined by the comparison of the free energy of the different solutions [17].

As already mentioned, in the most general case of the (0, 1/2, 1/2) superlattice, the compressible description requires the introduction of two independent secondary parameters ρ_1 and ρ_2 in addition to the primary order parameter m. Thus, the Landau free energy reads:

$$\Delta F = -J(\rho_1,\, \rho_2)m^2 - TS(m) + E_{\text{elas}}(\rho_1, \rho_2).$$

The three terms are respectively the "magnetic" (interaction), entropic and elastic contributions. Let us now consider a development of the different terms in power of the order parameters. The elastic energy is quadratic and with a proper definition of ρ_1 and ρ_2 we can write:

$$E_{\text{elas}}(\rho_1, \rho_2) = \frac{1}{2\chi_1}\rho_1^2 + \frac{1}{2\chi_2}\rho_2^2$$

where χ_1 and χ_2 are the compressibilities of the possible modes of distortion. In the same way, the interaction coupling constant J reads (up to quadratic order):

$$J(\rho_1, \rho_2) = J_0 + j_1\rho_1 + j_2\rho_2 + \eta_1\rho_1^2 + \eta_2\rho_2^2 + \gamma\rho_1\rho_2.$$

As ρ_1 and ρ_2 were defined to diagonalize the elastic energy, a cross term generally does exist in this development. Note that the η_i terms are small compared to the elastic energy and can thus be neglected. At this point, one may minimize the free energy relative to ρ_1 and ρ_2 to obtain

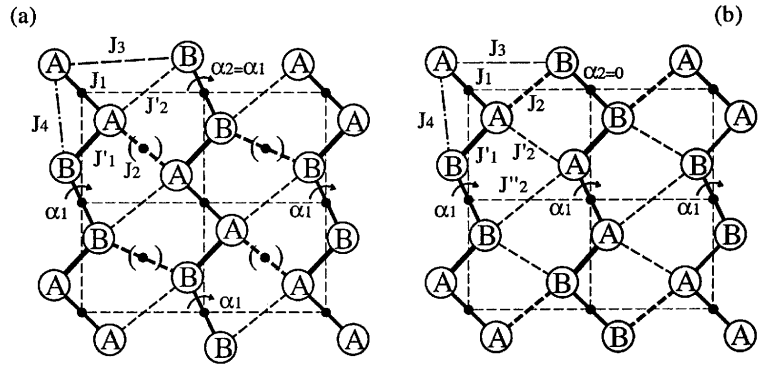

Fig. 15. (a) "Pseudo-centered" distortion in our simple model, (b) distortion for the (0, 1/2, 1/2) superlattice with molecular positions of Figure 14c (which shows the (0, 1/2, 0) distorted superlattice).

an effective free energy only dependent on the primary order parameter. One gets:

$$\Delta F_{\text{eff}}^{0,\,1/2,\,1/2} = -J_0 m^2 - TS(m) - \frac{1}{2}(\chi_1 j_1^2 + \chi_2 j_2^2)m^4 - \gamma\, j_1 j_2 \chi_1 \chi_2 m^6$$

where the entropy $S(m)$ can also be developed in power of m. The essential effect of the finite compressibilities is a renormalization of the fourth and sixth order terms in the development. The renormalization of the sixth order term is at the origin of the first-order line and of the liquid/gaz-like critical point [17]. The starting point for this discussion can be a development of the free energy which reads :

$$\Delta F_{\text{eff}}^{0,\,1/2,\,1/2} = A_2 m^2 + A_4 m^4 + A_6 m^6 + A_8 m^8.$$

Compared with the previous form of $\Delta F_{\text{eff}}^{0,\,1/2,\,1/2}$ the constant term $-TS(0)$ has been omitted. Figure 16a gives the plot of this function for representative values of the parameters (taking $A_8 = 1$ and $A_4 = 0.375$). The critical point is then obtained for $A_2 = -1/16$ and $A_6 = -1$. Note that this point is found as A_4 is still positive, *i.e.* when the renormalization of the sixth order term is the dominant effect. As a consequence, the model predicts at the same time a second-order phase transition (for $A_2 = 0$). This is in agreement with the experiment as the I-II phase transition line is always continuous. One finds the first-order transition line for special values of the parameters. When $A_8 = 1$, its equation reads:

$$A_2 = \frac{A_4 A_6}{2} - \frac{A_6^3}{8}.$$

Figure 16a also shows the typical shape of the free energy along this line. Far from the critical point, we quickly obtain an equilibrium between two phases with very different values of the order parameter, *i.e.* a strongly first order phase transition (see Fig. 16b). The small value of m in phase II (the equivalent of a gas) indicates a "quasi-centered" situation while a larger order parameter is found in phase III (equivalent to a liquid). The deduced theoretical phase diagram at this point of the discussion has the topology shown in Figure 16c. For simplicity we have kept A_4 constant considering that the main effect of alloying is to change A_6. A simultaneous modification of A_4 and A_6 would not change the topology. The main conclusion remains that the first order transition line is found as A_6 becomes more and more negative. To mimic the experimental phase diagram, it is quite natural to assume that the lattice compressibility changes with x and we conclude that the substitution of the smaller PF_6^- for AsF_6^- or SbF_6^- increases the renormalization of the sixth order term in the Landau development probably through an increase of the lattice compressibility.

In the competition with the (0, 1/2, 0) superlattice and because of the different wave-vector, different parameters should in principle be introduced. However, as we want to discuss the phase diagram topology far away from the critical point, *i.e.* when the II-IV or II-III phase transitions are strongly first order, we can use simplified arguments. As for a gas phase, we expect the entropic contribution to become quickly dominant in phase II. As the order parameter at thermal equilibrium becomes small, we can write $\Delta F_{\text{eff}}^{\text{II}} \simeq -TS(0)$ (omitting the small correction coming from the finite but small value of m). In the same way, "enthalpic" (interaction) terms are essential to describe phases III and IV. The order parameter can thus be considered as almost saturated (equal to 1 with a proper normalization). We have for example:

$$\Delta F_{\text{eff}}^{\text{III}} \simeq -J_0 - \frac{1}{2}(\chi_1 j_1^2 + \chi_2 j_2^2) - \gamma j_1 j_2 \chi_1 \chi_2.$$

A similar expression would be obtained for $\Delta F_{\text{eff}}^{\text{IV}}$ with different coefficients. At this approximation, $\Delta F_{\text{eff}}^{\text{III}}$ and $\Delta F_{\text{eff}}^{\text{IV}}$ are only functions of x (through the dependence of the compressibilities with the anion size). Following this argument, the equation of the III-IV transition line reads $\Delta F_{\text{eff}}^{\text{III}} = \Delta F_{\text{eff}}^{\text{IV}}$, *i.e.* it is a vertical line in the (x, T) plane. In the same way, the equation for the II-III and II-IV transition lines are respectively:

$$T = -\frac{\Delta F_{\text{eff}}^{\text{III}}}{S(0)} \quad \text{and} \quad T = -\frac{\Delta F_{\text{eff}}^{\text{IV}}}{S(0)}.$$

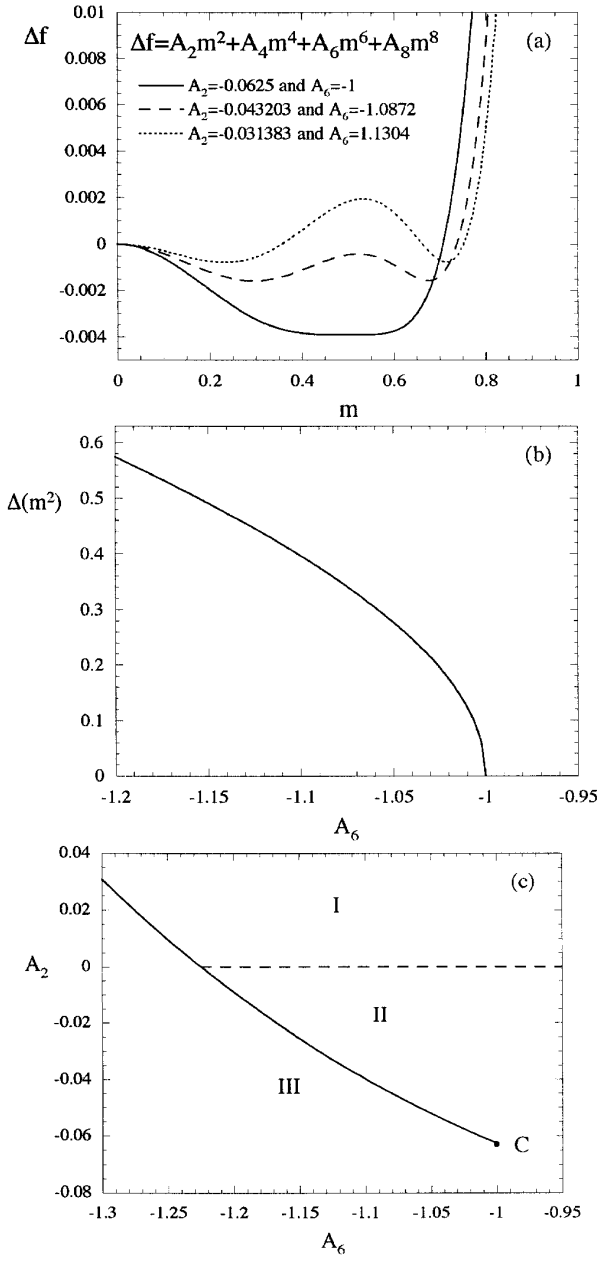

Fig. 16. (a) Landau free energy of the (0, 1/2, 1/2) superlattice for selected A_6, A_2 values and for $A_4 = 0.375$ and $A_8 = 1$, (b) discontinuity of the square of the order parameter along the first order line ($\Delta(m^2) = m_2^2 - m_1^2$ where m_1 and m_2 are the values of the order parameter for the two phase in equilibrium), (c) deduced phase diagram in (A_6, A_2) space for $A_4 = 0.375$ and $A_8 = 1$ (the continuous line is first order while the dashed line is second order).

They may be almost horizontal lines if the free energies $\Delta F_{\text{eff}}^{\text{III}}$ and $\Delta F_{\text{eff}}^{\text{IV}}$ are only weakly dependent on the anion size.

In conclusion, the above discussion explains the main characteristics of the experimental phase diagram. The major argument is the need for a compressible model. Moreover, we have shown that the combination of two independent modes of distortion brings the observed distinctive topology of the phase diagram. Finally, the (0, 1/2, 0) superlattice is stabilized for enthalpic reasons, for example when the lattice compressibility becomes large enough. It is also important to note that the above theoretical arguments are independent of microscopic details which would however be relevant to discuss the structure of the phase diagram in more details.

4 Concluding remarks

We have investigated in this paper the physical properties of two series of solid solutions. This was the experimental answer for a better understanding of the physical properties of the $[Cp_2Mo(dmit)^{+\bullet}][X^-]$ salts, and particularly their low temperature structural phase transitions. The room temperature crystal structure of these materials shows that the octahedral anions are statistically disordered. A possible ordering may explain why the room temperature orthorhombic symmetry is not preserved upon cooling. As a consequence, a complex phase diagram is found in these series with the possibility of several successive structural phase transitions.

The understanding of these instabilities is important as the electronic properties (for example the low temperature magnetic ordering) depends on the interactions and therefore on the crystal structure. Although the low temperature structure is missing, we have proposed a Landau theory to explain the phase diagram. The main argument is the need for a compressible model, the liquid/gaz-like critical point found in one of the low symmetry phases being explained by the coupling with two modes of distortion. Only a few examples of solids of this kind have been described experimentally [17] although similar arguments have been used to modelize the phase diagram of surfactants in solution [18]. Finally it should also be noted that these materials are among the few organic materials where a disorder of centrosymmetrical anions have been reported [19].

As a general property among the series, the magnitude of the magnetic exchange interactions is worthnoting. One consequence is the systematic occurrence of a low temperature antiferromagnetic ground state. This new series may thus be the starting point for the discovery of new materials with attractive electronic properties.

In the future, it would be interesting to study new materials with anions of different symmetry and compare their crystal structure and physical properties with the one of the present salts. The other substitution may concern the cation radical itself where oxygen or selenium atoms may be substituted for one or several sulfur atoms of the $dmit^{2-}$ ligand.

We thank F. Grelaud and D. Lepevelen (ICMCB, Pessac) for their participation to low temperature X-ray diffraction and

J. Amiell (CRPP, Pessac) for his invaluable technical help during EPR experiments. Discussions with J.-P. Pouget (LPS, Orsay) and P. Batail (IMN, Nantes) are also gratefully acknowledged. Finally, we thank F. Gritti and N. Kinoshita for their participation during a short stay in the laboratory.

References

1. R. Clérac, M. Fourmigué, J. Gaultier, Y. Barrans, P.A. Albouy, C. Coulon, Eur. Phys. J. B **9**, 431 (1999).
2. V. Ilakovac, S. Ravy, K. Boubekeur, C. Lenoir, P. Batail, J.P. Pouget, Phys. Rev. B **56**, 13878 (1997).
3. V. Ilakovac, S. Ravy, J.P. Pouget, C. Lenoir, K. Boubekeur, P. Batail, S. Dolanski Babic, M. Biskup, B. Korin-Hamzic, S. Tomic, C. Bourbonnais, Phys. Rev. B **50**, 7136 (1984).
4. R. Laversanne, C. Coulon, J.P. Pouget, R. Moret, J. Phys. Lett. **45**, 393 (1984).
5. A.K. Pal, Indian J. Pure Appl. Phys. **34**, 681 (1996).
6. C. Coulon, P. Delhaès, S. Flandrois, R. Lagnier, E. Bonjour, J.M. Fabre, J. Phys. France **43**, 1059 (1982).
7. R. Laversanne, J. Amiell, P. Delhaès, D. Chasseau, C. Hauw, Solid State Commun. **52**, 177 (1984).
8. Strictly speaking, phases III and IV have the same symmetry but a phase transition between these two phases will be generally observed: see for example Y. Park, T.C. Lubensky, P. Barois, J. Prost, Phys. Rev. A **37**, 2197 (1988).
9. P.M. Chaikin, T.C. Lubensky, *Principles of condensed matter physics* (Cambridge University Press, 1995).
10. C. Coulon, J.C. Scott, R. Laversanne, Phys. Rev. B **33**, 6235 (1986).
11. T. Nagamiya, K. Yosida, R. Kudo, Adv. Phys. **4**, 1 (1954).
12. T. Nagamiya, Proj. Theor. Phys. **11**, 309 (1954).
13. L.P. Kadanoff, W. Götze, D. Hamblen, R. Hecht, E.A.S. Lewis, V.V. Palciauskas, M. Rayl, J. Swift, Rev. Mod. Phys. **39**, 395 (1967).
14. M. Blume, V.J. Emery, R.B. Griffiths, Phys. Rev. A **4**, 3 (1971).
15. D. Mukamel, M. Blume, Phys. Rev. A **10**, 2 (1974).
16. M. Roger, J.M. Delrieu, E. Wope-Mbougue, Phys. Rev. B **34**, 4952 (1986).
17. J.C. Tolédano, P. Tolédano, *The Landau theory of phase transitions* (World Scientific Publishing Compagny, 1987).
18. D. Roux, C. Coulon, M.E. Cates, J. Phys. Chem. **96**, 4174 (1992).
19. Anion ordering has been extensively studied in Bechgaard salts with anions of lower symmetry. See for example: J.P. Pouget in *Low-dimensional conductors and superconductors* (NATO ASI series, edited by D. Jérome and L.G. Caron, Plenum Press, New York, 1987), p. 17.